Carbon 222 (2024) 118906

Contents lists available at ScienceDirect

Carbon

journal homepage: www.elsevier.com/locate/carbon

Localized states in carbon dots: Structural and optical investigation of three systems with varying degrees of carbonization

Keenan J. Mintz [a,b], Claude Poleunis [c], Braulio C.L.B. Ferreira [a], Rachel Sampson [a], Arnaud Delcorte [c], Roger M. Leblanc [a,*]

[a] Department of Chemistry, University of Miami, Coral Gables, FL 33146, USA
[b] School of Materials Science and Engineering, Georgia Institute of Technology, Atlanta, GA 30332, USA
[c] Institute of Condensed Matter and Nanoscience, Université Catholique de Louvain, 1348 Louvain-la-Neuve, Belgium

ARTICLE INFO

Keywords:
Carbon dots
Time of flight-Secondary ion mass spectrometry
Localized states
Photoluminescence mechanism

ABSTRACT

Carbon dots (CDs) have been widely researched in recent years, mainly to investigate their potential in various applications such as drug delivery, photocatalysis, and sensing. However, understanding of their fundamental properties, including physical and electronic structure, has lagged behind their development in applied sciences. To address this, it is necessary to use novel methods which go beyond the current level of characterization in the literature. In this work, we utilize time of flight-secondary ion mass spectrometry (ToF-SIMS) to generate specific knowledge of the structural components of three CDs generated in our lab. This work revealed that black CDs (B-CDs) possess a highly carbonic structure with nitrogen and oxygen functionalization throughout the particle structure. Carbon nitride dots (CNDs) possess some of these same carbonic structures, but also show the presence of more organic structures which would be expected through a bottom-up approach. In terms of carbonization, CNDs lie between B-CDs and the third sample, yellow-CDs (Y-CDs). Y-CDs are believed to be almost completely polymeric/organic in structure and the groups detected through this mass analysis supports this idea. The structural information from ToF-SIMS is compared with other structural techniques. Additionally, the optical properties of CDs before and after oxidation and reduction are used to craft a proposed photoluminescence (PL) mechanism for each system. The analysis contained herein enables further understanding of the structure of these three samples, and the attained understanding of the surface structure is particularly important for future biomedical applications.

1. Introduction

Carbon dots (CDs) have been well investigated in recent years for a variety of promising applications [1]. These applications include drug delivery [2,3], bioimaging [4,5], photocatalysis [6,7], and the sensing of ions and biomolecules [8,9]. This extensive research has shown the large potential of CDs in various areas, but CDs are often limited in the optimization of their ability due to the fact that they are poorly defined structurally and electronically. This lack of clarity often hinders the ability to precisely modify and improve CDs in a specific way. Furthermore, to develop CDs in nanomedicine with the potential to apply them in treatment of humans, it is necessary to have a clear understanding of the structure of CDs [10,11]. This is especially true for the surface structure of CDs since this will largely determine the interactions of CDs in a biological system.

The structure of CDs has been unclear in many systems for many years, but in recent years the necessary investigation has begun [12]. Otyepka and coworkers used computational methods to develop and assess the feasibility of a structure for CDs involving the stacking of sp^2 lattices [13]. This has been proposed for other systems as well, especially those labeled as graphene quantum dots [14]. For CDs prepared through top-down approaches and bottom-up approaches with sufficient energy to induce graphitization, it is clear that sp^2 lattices are the main factor in the formation of CDs' core [15]. Recently we developed a 3D model for two CDs systems in our lab which possess a largely sp^2 hybridized core structure [16]. Due to the wide variations in the preparation methods of CDs, there is, however, other structures which may be important for different systems. A hybrid sp^2/sp^3 system has been observed for different CDs, including one system from our lab [16,17]. Recently Russo et al. extracted carbon particulate from a flame reactor which was

* Corresponding author.
E-mail address: rml@miami.edu (R.M. Leblanc).

https://doi.org/10.1016/j.carbon.2024.118906
Received 6 August 2023; Received in revised form 13 December 2023; Accepted 6 February 2024
Available online 14 February 2024

then rigorously separated through an SEC column. The authors found that CDs with smaller molecular weights possessed blue emission which was most likely the result of small molecules. Larger CDs showed longer wavelength emission and the structure in these cases was believed to be mostly related to oligomeric aromatic hydrocarbons [18]. The multitude of precursors and preparation methods for CDs compels deep structural investigation of each type of system in order to obtain a clear understanding of their structure.

The recent advances in the structures of CDs have provided information concerning the core and surface of CDs, but their structure is still most often described in generalities. Techniques such as Fourier-transform infrared (FTIR) and X-ray photoelectron (XPS) spectroscopies can provide the types of functionalities present in CDs but may not provide specific structural information and will definitely not allow for the determination of exact structures. Time of flight-secondary ion mass spectrometry (ToF-SIMS) can provide the information to create a more detailed structure for CDs. This technique utilizes a beam of ions (primary ions) focused on a sample to break off layers of the surface as small as 1 nm (secondary ions) which can then be detected through a time of flight mass analyzer [19]. The depth of penetration depends on the nature and energy of the applied primary ion beam and on the nature of the sample [20]. This provides precise masses which can be correlated to structural moieties present in the sample. This has begun to be applied to CDs in recent years, but only in a very cursory manner and this is the first work to present and analyze in-depth results from this technique for CDs [21,22].

Another highly debated property of CDs is their photoluminescence (PL) mechanism. The excitation-wavelength dependent (tunable) emission and high quantum yields for CDs makes them exciting candidates for the applications described above, but there is much that is still not known about this phenomenon. A few popular interpretations of the PL mechanism of CDs are quantum confinement (size dependent emission), surface states (arising from energy traps), and molecular states (from attached small molecules) [23,24]. Since CDs are a broadly defined material, there is some evidence to support each of these hypotheses, but it is clear that some are more relevant than others. Most CDs do not have data to support a quantum confinement effect, which is unsurprising given that the structures of CDs are significantly different from metal-based quantum dots [24,25]. Conversely there has been some very detailed work showing the presence of small molecule fluorophores in CDs for some methods, especially those based on citric acid [26]. The most commonly applied mechanism for CDs' PL properties is related to "surface states", which is a concept which is very well defined for solid state semiconductors [27,28]. There is significant evidence for this type of process, but we would argue it is better to extrapolate CDs' properties from concepts found in the electronic states of carbon materials as opposed to inorganic semiconductors. For this reason, we analyze our CDs in this paper through the paradigm of localized states which have been well defined for various carbon materials previously [29,30]. More recently, scientists have begun to apply this concept to CDs [31,32]. Shan and coworkers developed ultrabright yellow emissive CDs which the authors attributed to localized electronic states. Nitrogen doping enhanced this emission further by allowing for typically forbidden transitions to occur. The many examples of CDs' emission being attributed to surface states in the literature may benefit from a reexamination with a more accurate model of localized states based on carbon materials.

This work is an effort to build on our previous paper and provide a more detailed structural model for the previously investigated three systems [16]. Black CDs (B-CDs) are prepared through a top-down approach and have shown promise in preventing peptide fibrillation and in drug delivery [3,33]. Carbon nitride dots (CNDs) represent a bottom-up approach which undergoes a significant amount of graphitization. These have also shown promise in different areas of drug delivery as well as bioimaging [5,34]. The third system is related to yellow CDs (Y-CDs) which are prepared through a bottom-up approach with little graphitization and have been utilized by our lab in 3D printing and different biological applications [35,36]. These systems represent a large portion of CDs literature in terms of precursors and degree of carbonization. Our previous work to develop an initial structural model was compelled by the strong promise of these CDs in nanomedicine. In this work we utilize ToF-SIMS to provide a more detailed picture of the structure of each system. This novel technique is compared with more standard techniques of XPS and elemental analysis in order to enable their optimization and their potential realization in nanomedicine for treatment of disease in humans. Furthermore, the structural information obtained is compared with the optical properties of CDs before and after modification in order to generate a proposed PL mechanism.

2. Materials and methods

2.1. Preparation of CDs

The preparation of these three systems has been previously described in detail and the most important details will be mentioned here for clarity [16]. As mentioned previously, B-CDs are prepared through a top-down approach involving the treatment of carbon nanopowder with sulfuric and nitric acids and refluxing for 15 h at 110 °C. The reaction mixture is then neutralized with NaOH and vacuum filtered to remove unreacted carbon and sodium salts. The mixture is then washed with chloroform three times, followed by dialysis in a membrane possessing a molecular weight cutoff (MWCO) of 3500 Da. CNDs are prepared from a microwave-mediated approach. Citric acid and urea are combined in a 1:1 mass ratio, stirred overnight at room temperature, and heated in a domestic microwave oven at 700 W for 7 min. Purification for CNDs involves two rounds of centrifugation to remove large particles, syringe filtration (0.2 μm) to remove finer particles, and dialysis (MWCO 100–500 Da) to remove any unreacted small molecules. Y-CDs are prepared from citric acid and *o*-PDA (1:25 M ratio) treated with ultrasonication (42 kHz) for 1 h. The solution was then cooled in an ice bath to remove unreacted *o*-PDA. The mass of unreacted *o*-PDA was 0.127 g which indicates that 0.433 g participated in the reaction. This created an effective molar ratio between citric acid and *o*-PDA of 1:19. The CDs were then purified with size exclusion chromatography (SEC) using Sephacryl S-300 as the stationary phase and DI water as the mobile phase.

2.2. Oxidation/reduction of CDs

To perform oxidation of CDs, 25 mg of CDs was dissolved in 5 mL water and 0.37 mL of 10% NaOCl solution was added. The mixture was then stirred for 1 h at room temperature. Following this reaction, the solution was then dialyzed for 2 days (MWCO 100–500 Da) to remove unreacted salts and hypochlorite. The solution was then lyophilized to obtain oxidized CDs (O-CDs). To perform reduction of CDs, 25 mg of CDs was dissolved in 5 mL water and 18.92 mg of $NaBH_4$ was added. The mixture was then stirred for 1 h at room temperature. After the reaction, the solution was then dialyzed for 2 days (MWCO 100–500 Da) to remove unreacted salts and borohydride. The solution was then lyophilized to obtain reduced CDs (R-CDs).

2.3. Instrumentation

Chemical characterisation of samples were carried out by using a TOF-SIMS instrument (IONTOF GmbH, Münster, Germany). Before measuring the samples, a precleaning of the measured surfaces was done by an Ar gas cluster ion beam (Ar-GCIB) used as sputtering source. The Ar-GCIB ion source was operated at 5 keV with a direct current of 600 pA. The Ar-GCIB cluster distribution was centered on Ar^{+}_{5000}. For the precleaning of the surface, the focused Ar-GCIB beam of primary ions was rastered over an area of 600 x 600 μm^2. The total pre-cleaning dose was $7x10^{12}$ $Ar^{+}_{5000}.cm^{-2}$. Then, a pulsed Bi^{+}_{5} liquid metal ion source was used

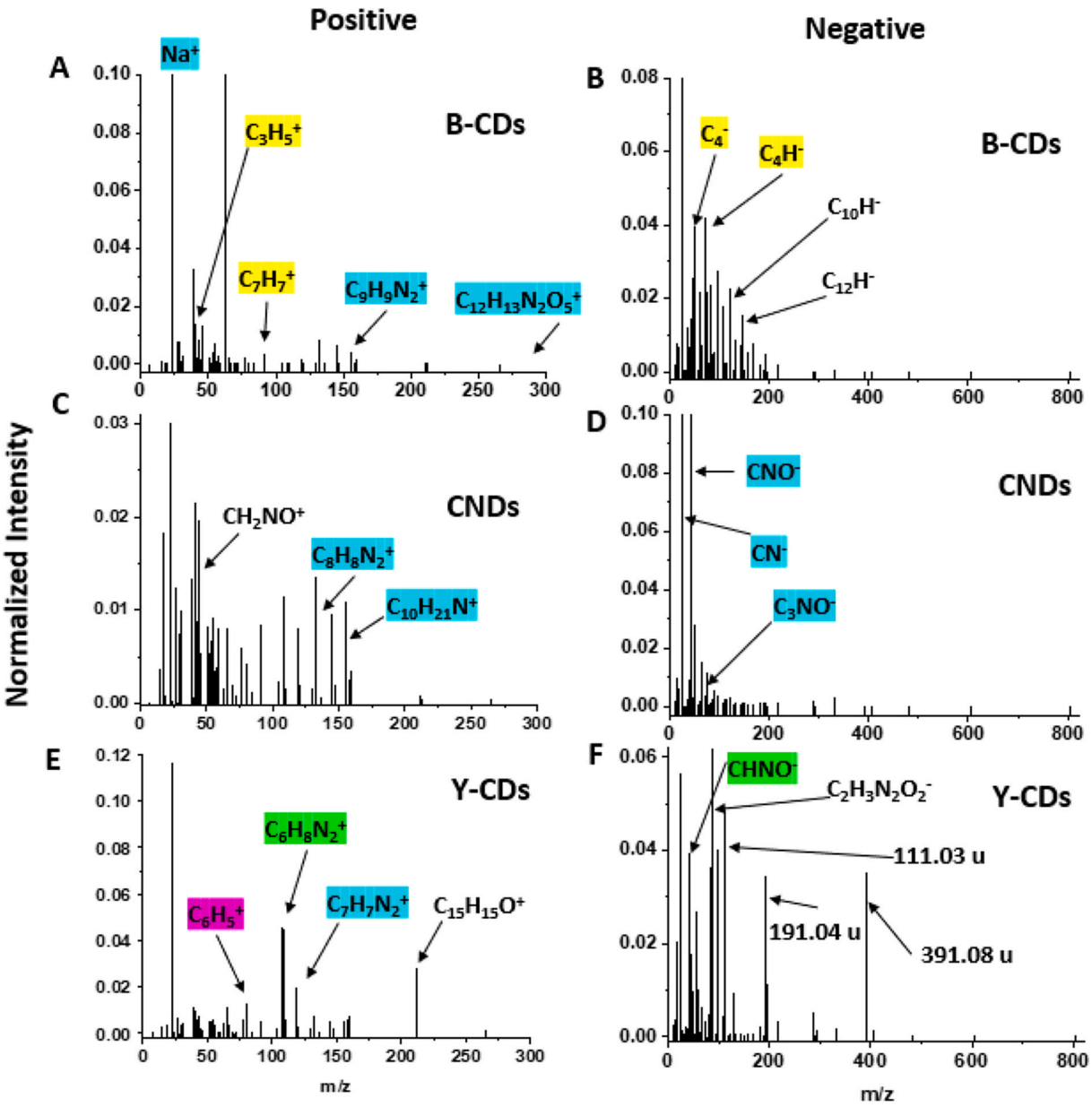

Fig. 1. Secondary ion mass spectra for B-CDs (A,B), CNDs (C,D), and Y-CDs (E,F) in positive (left) and negative (right) polarity after ionization with a Bi_5^+ ion beam. Normalization is performed by dividing peak intensity by the total area of the entire spectrum. Structures in blue indicate the ion is among the top twenty most abundant peaks in all three samples, yellow indicates it is shared by just B-CDs and CNDs, purple shows the common features between B-CDs and Y-CDs, and green marks the ions common to CNDs and Y-CDs. More detailed labeling of peaks can be found in Tables S1 and S2.

to produce a primary beam using an acceleration voltage of 30 kV. An alternating target current of 0.04 pA with a bunched pulse width lower than 1 ns was used. Both positive and negative secondary ion species were analysed. For spectra, a raster of 128 x 128 data points over an area of 200 × 200 μm [2] was used. The total primary ion beam dose for each analysed area was always kept below $4x10^{10}$ ions.cm^{-2}, ensuring static conditions. For the Bi^+ measurements, the a.c. target current was 1 pA, and the total primary ion beam dose was $1x10^{12}$ ions.cm^{-2}. Lateral resolution of ~3 μm and mass resolution m/Δm > 4500 at 29 *m/z* were maintained for positive and negative spectra acquisition. Fig. S1 practically illustrates the resolution which can be obtained with this technique. Charge compensation was done by an interlaced electron flood gun (E_k = 20 eV). All data analyses were carried out using the software supplied by the instrument manufacturer, SurfaceLab (version 6.8). Sample powders were pressed onto adhesive part of Post-it® papers. Fig. S2 shows that the powder covered over the whole analysis area and that sampling of the adhesive was not going to occur.

UV–vis spectra were measured with an Agilent Cary 100 UV–vis spectrophotometer on aqueous dispersions of CDs (0.1 mg/mL). PL characterization was performed on a Fluorolog HORIBA Jobin Yvon fluorometer with a slit width of 5 nm for both excitation and emission and a concentration of 0.01 mg/mL of CDs in DI water. All optical characterization spectra were obtained with quartz cells possessing a pathlength of 1 cm. The attenuated total reflection Fourier-transform infrared (ATR-FTIR) spectra were obtained for solid CDs powders with a FTIR spectrometer (FT-Nicolet 5700, Thermoscientific) equipped with a Smartorbit (Thermoscientific) operating in attenuated total reflectance (ATR) in a range between 600 and 4000 cm^{-1}. Elemental analysis was conducted by Intertek Pharmaceutical Services on CDs powders.

3. Results and discussion

3.1. Time of flight secondary ion mass spectrometry (ToF-SIMS) analysis

The multitude of peaks seen in Fig. 1 immediately communicates the diversity of surface groups on CDs' structural components. More than 100 peaks can be seen above the background for the three samples, with varying intensities between the different samples. Figs. S3 and S4 show the measured counts normalized by the total counts of the mass spectrum. The noise level is very low below *m/z* 20 and increases up to 100–1000 counts beyond *m/z* 100, but the signal to noise is still low ($\sim 10^3$). It is interesting to note the similarities and differences between samples. The most intense peaks are summarized in Tables 1 and 2 and similar tables are given in Tables S1 and S2 with color coding to easily indicate commonality between the samples. Some observed masses correspond to species associated with CDs purification (e.g., Na^+, K^+, etc.). Of the top twenty masses for B-CDs, the most common structures are hydrogenated carbon in positive polarity (C_xH_y) and pure carbon in negative polarity (C_x). Due to the higher degree of graphitization in CNDs compared to Y-CDs, CNDs shares much more similarity with B-CDs. Upon first examination, the general trend we would expect based on the precursors/preparation methods can be seen, but there is also some surprising information which can be obtained through a closer investigation of the individual data sets.

As mentioned above, many of the most important masses for B-CDs involve pure carbon/hydrogenated carbon, but some involve nitrogen and oxygen as well (Fig. 1A and **B**, Tables 1 and 2). It is somewhat surprising that oxygen is not more prevalent considering the elemental ratios which have been measured from XPS (Table 3), although caution must be exercised when interpreting intensities from SIMS data [16,33]. Conversely, nitrogen is present to a greater extent than expected, which must originate through the use of nitric acid in the preparation process. The large presence of carbon structures is not surprising considering the carbon nanopowder precursor, and these results indicate the functionalization of B-CDs is enough to produce the high water dispersibility of these particles, but still the fringes of the carbon lattices dominate the structure of B-CDs. As will be discussed below, there are specific peaks which show higher relative intensity for CNDs and Y-CDs, but B-CDs shows a more even distribution across the detected masses (Tables 1 and 2). This is exactly what is expected for these particles since they are prepared from a larger carbon particle and the peaks measured are simply the distribution of how B-CDs breaks apart due to the primary ion beam.

CNDs share many similarities with B-CDs as seen from the comparison in Tables S1 and S2 (blue and yellow colors). This balance between the two more extreme structures (carbonized for B-CDs versus organic for Y-CDs) is what would be expected for the relatively harsh bottom-up approach for CNDs. Urea and citric acid are not directly observed due to the carbonization process in CNDs preparation. A majority of the most intense ion peaks correspond to structures containing nitrogen, supporting the importance of nitrogen-doping for this system. Ions such as $C_3HN_2^-$ and C_3NO^- are formed due to urea self-reaction and with citric acid. NH_4^+ presence in CNDs is also due to urea. The presence of larger masses shows that the polymer, which is prepared through overnight stirring of the precursors, does not completely carbonize upon microwave treatment and remains as a surface organic structure. The functionality with six carbon or more may play an important role in the PL properties of CNDs, as several studies have shown evidence for organic fluorophores being responsible for some of the PL properties of citric acid-based CDs. Significant amounts of phenylenediamine related peaks ($C_6H_8N_2^+$ and $C_6H_9N_2^+$) confirms the aromatization of the precursors in the preparation process. Of the three particles, CNDs are expected to be the most heterogenous composition of structures based on our previous work with TLC separation [37]. Thus, the diverse structures from sample could from different types of particles or there is a significant difference in surface polarity among the CNDs.

Table 1
Formula and masses of the most intense ion peaks detected for B-CDs, CNDs, and Y-CDs with a positive polarity using a Bi_5^+ ion beam. Cells highlighted in red indicates that the ion peak is among the twenty most abundant for that particular sample.

		Percentage of total signal		
	Mass (u)	B-CDs	CNDs	Y-CDs
CH_3^+	15.0235	0.14	0.37	0.29
NH_4^+	18.0355	0.02	1.83	0.40
H_3O^+	19.0179	0.02	0.07	0.11
Na^+	22.9919	16.75	3.00	11.60
$C_2H_3^+$	27.0231	0.79	1.24	0.69
CHO^+	29.0024	0.12	0.38	0.25
$C_2H_5^+$	29.0463	0.75	0.74	0.39
NO^+	29.993	0.03	0.02	0.00
CH_4N^+	30.038	0.09	0.71	0.39
CH_3O^+	31.0176	0.29	0.98	0.44
CH_5N^+	31.0421	0.01	0.04	0.01
K^+	38.9666	3.29	1.34	1.08
$C_3H_5^+$	41.0394	1.42	2.15	1.02
$C_2H_4N^+$	42.0389	0.23	0.98	0.61
$C_2H_3O^+$	43.0198	0.27	0.88	0.73
$C_3H_7^+$	43.0641	0.85	0.86	0.42
CH_2NO^+	44.0129	0.13	1.97	0.22
$C_2H_6N^+$	44.051	0.14	0.34	0.15
CHO_2^+	44.9965	0.01	0.03	0.13
$C_2H_5O^+$	45.036	0.25	0.55	0.21
CH_4NO^+	46.0315	0.03	0.08	0.01
$C_2H_8N^+$	46.0678	0.03	0.09	0.05
$C_4H_3^+$	51.0235	0.21	0.82	0.51
$C_3H_2N^+$	52.0129	0.06	0.53	0.34
C_3HO^+	53.0019	0.42	0.36	0.10
$C_4H_5^+$	53.037	0.33	0.67	0.54
$C_3H_4N^+$	54.0362	0.11	0.66	0.57
$C_3H_3O^+$	55.0206	0.13	0.91	0.19
$C_4H_7^+$	55.0667	0.73	0.82	0.39
$C_3H_6N^+$	56.0527	0.11	0.35	0.19
$C_3H_8N^+$	58.0856	0.28	0.38	0.08
$C_3H_7O^+$	59.0438	0.06	0.81	0.05
Na_2OH^+	62.9883	12.37	0.15	0.47
$C_5H_5^+$	65.0379	0.22	0.81	1.14
$C_4H_4N^+$	66.0375	0.06	0.40	0.38
$C_4H_5O^+$	69.0344	0.03	0.20	0.08
$C_3H_4NO^+$	70.0316	0.03	0.18	0.02
$C_4H_{10}N^+$	72.0865	0.02	0.09	0.03
$C_6H_5^+$	77.037	0.20	0.59	0.58
$C_5H_6N^+$	80.05	0.07	0.42	1.27
$C_4H_6NO^+$	84.0426	0.02	0.11	0.02
$C_7H_7^+$	91.0544	0.35	0.83	0.50
$C_3H_8N_2O_2^+$	104.052	0.06	0.23	0.22
$C_6H_8N_2^+$	108.0711	0.06	1.02	4.59
$C_6H_9N_2^+$	109.0799	0.05	1.14	4.46
$C_6H_{10}N_2^+$	110.1119	0.03	0.16	0.60
$C_7H_7N_2^+$	119.0848	0.17	0.79	1.97
$C_4H_{12}N_2O_2^+$	120.0887	0.04	0.19	0.30
$C_9H_8N^+$	130.0699	0.04	0.16	0.22
$C_8H_8N_2^+$	132.0721	0.84	1.35	0.69
$C_9H_9N_2^+$	145.0761	0.61	0.96	0.53
$Si_2OC_5H_{15}^+$	147.0853	0.08	0.20	0.20
$C_{10}H_{21}N^+$	155.1609	0.41	1.08	0.52
$C_{10}H_{10}N_2^+$	158.0842	0.05	0.24	0.60
$C_{10}H_{11}N_2^+$	159.0935	0.14	0.35	0.78
$C_{15}H_{15}O^+$	211.1028	0.06	0.07	2.83
$C_{15}H_{16}O^+$	212.116	0.02	0.04	2.25

Table 2
Formula and masses of the most intense ion peaks detected for B-CDs, CNDs, and Y-CDs with a negative polarity using a Bi_5^+ ion beam. Cells highlighted in red indicates that the ion peak is among the twenty most abundant for that particular sample.

		Percentage of total signal		
Formula	**Mass (u)**	**B-CDs**	**CNDs**	**Y-CDs**
C^-	12.0009	0.19	0.21	0.24
CH^-	13.0088	0.34	0.32	0.38
NH^-	15.0114	0.00	0.02	0.01
O^-	15.9959	0.79	0.97	1.68
OH^-	17.004	0.67	0.61	2.05
C_2^-	24.0021	0.84	0.39	0.42
C_2H^-	25.0114	2.82	1.39	1.91
CN^-	26.0102	8.12	14.40	5.64
$^{13}CN^-$	27.0074	0.13	0.22	0.15
CHO^-	29.0047	0.00	0.01	0.02
NO^-	29.9983	0.01	0.01	0.00
CH_3O^-	31.021	0.01	0.02	0.03
O_2^-	31.9976	0.03	0.01	0.04
C_3^-	36.0017	1.17	0.25	0.20
C_3H^-	37.0103	0.37	0.13	0.17
C_2O^-	39.998	0.24	0.17	0.18
C_2HO^-	41.0049	0.70	0.92	2.80
CNO^-	42.0119	1.47	17.81	1.86
$CHNO^-$	43.0049	0.13	0.33	3.91
CHO_2^-	45.0007	0.35	0.74	1.76
NO_2^-	45.9978	1.00	0.02	0.03
C_4^-	48.0003	2.54	0.32	0.18
C_4H^-	49.0102	3.93	0.75	0.52
C_3N^-	50.0075	3.10	2.80	0.98
$C_3H_2N^-$	52.022	0.03	0.13	0.04
$C_2H_5N_2^-$	57.041	0.01	0.02	2.67
$C_2H_2O_2^-$	58.0073	0.02	0.03	0.21
$C_2H_3O_2^-$	59.0209	0.04	0.07	0.99
C_5^-	59.9996	2.19	0.21	0.11
C_5H^-	61.0167	0.91	0.14	0.24
$C_3HN_2^-$	65.0132	0.69	0.89	0.63
C_3NO^-	66.0043	0.68	1.56	0.38
C_6^-	72.0012	3.28	0.22	0.08
C_6H^-	73.0094	4.20	0.40	0.28
C_5N^-	74.0059	2.18	1.13	0.31
C_7^-	84.0046	2.38	0.16	0.09
$C_3H_5N_2O^-$	85.0444	0.50	0.05	3.61
$C_2H_3N_2O_2^-$	87.0191	0.23	0.26	6.18
$C_5HN_2^-$	89.026	0.51	0.57	0.28
C_8^-	96.0046	2.71	0.38	0.05
C_9^-	108.0034	1.78	0.11	0.06
109.00 u	108.9957	1.02	0.13	0.42
111.03 u	111.0296	0.25	0.22	4.81
113.01 u	113.0138	0.23	0.28	0.82
C_{10}^-	120.0006	1.09	0.16	0.02
$C_{10}H^-$	121.014	2.27	0.16	0.04
C_9N^-	122.0073	0.87	0.28	0.05
129.04 u	129.0358	0.02	0.06	0.94
C_{11}^-	132.0017	0.86	0.09	0.05
C_{12}^-	143.9971	0.73	0.05	0.01
$C_9H_6NO^-$	144.0644	0.29	0.08	0.02
$C_{12}H^-$	145.0122	1.53	0.10	0.06
C_{13}^-	155.9989	0.54	0.06	0.05
$C_{14}H^-$	169.011	0.79	0.08	0.07
$C_8H_7SO_3^-$	183.0126	0.19	0.11	0.20
188.03 u	188.0348	0.02	0.14	0.02
191.04 u	191.0355	0.03	0.14	3.43
$C_{16}H^-$	193.0099	0.48	0.11	0.09
194.94 u	194.9411	0.02	0.02	1.14
217.04 u	217.0364	0.20	0.11	0.30
287.04 u	287.0401	0.01	0.06	0.53
292.92 u	292.9241	0.01	0.03	0.14
331.04 u	331.0417	0.01	0.04	0.20
333.07 u	333.0662	0.01	0.30	0.03
391.08 u	391.0764	0.01	0.02	3.50
405.07 u	405.066	0.01	0.01	0.14
481.13 u	481.1313	0.00	0.01	0.05

Y-CDs predictably show the most seemingly organic structural features (Fig. 1E and **F**, Tables 1 and 2). Interestingly, it seems that *o*-PDA is directly responsible for the two most intense peaks ($C_6H_8N_2^+$ and $C_6H_9N_2^+$) for Y-CDs measured in a positive polarity, which supports the structure proposed for this system previously [16]. There are also two peaks with a mass to charge ratio between 190 and 195 which are most likely due to citric acid moieties present in the final structure of Y-CDs. Overall, larger masses dominate the spectra for Y-CDs compared to the other two particles. This is most likely due to the highly polymeric nature of this system, as the larger masses from B-CDs are exclusively related to carbon structures. The lack of carbonization can also be clearly seen for Y-CDs as the intensities of peaks related to $C_xH_y^+$ and C_x^- structures are relatively low compared to B-CDs and CNDs. Y-CDs also shows the highest amount of oxygen (from O^- and H_3O^+) which is contradictory to results seen from XPS and elemental analysis (Table 3). This is most likely due to the more hygroscopic nature of Y-CDs.

To further probe the results obtained from this method, different primary ion conditions were utilized. The results discussed above were obtained using a Bi_5^+ ion beam, and in addition to this, a Bi^+ beam was used which was a gentler ionization which resulted typically results in less damage to the sample. A third method involved a gentle sputtering of argon to remove any potential surface contaminants before measuring SIMS data with Bi_5^+ ion beam. The comparison of these datasets is found in (Tables S1–S4, Fig. S5). When Y-CDs were measured after precleaning (Tables S5-S6), the oxygen content is reduced indicating that loosely bound water had been removed from the sample by the argon sputtering. For most masses, these datasets show the same patterns, indicating no contaminants or loosely bound surface groups. There are some changes in intensity, for example, large differences are seen for the larger masses detected for Y-CDs. These are most likely related to organic oligomers which may be removed to a greater extent by the argon sputter precleaning compared to the more carbonized structures of B-CDs and CNDs.

3.2. Comparison of ToF-SIMS with XPS and elemental analysis

More standard characterization can be used to further shed light on the structure of CDs and also help to interpret surface/core structures. XPS is known for being surface sensitive, although CDs are small enough that XPS most likely can penetrate throughout the particle. However, it is believed that the quantitative response is biased to the surface, hence the values in Table 3 do not necessarily reflect the whole particle composition of CDs [38]. More similar composition is seen between B-CDs and CNDs compared to Y-CDs. B-CDs, possesses the most similarity between the two techniques indicating that its composition is relatively uniform throughout the particle, which also correlates with the SIMS data. This is unsurprising given the top-down approach used to prepare B-CDs. The main difference for B-CDs is the enhancement of oxygen from elemental analysis relative to carbon. This indicates that the interior lattices of B-CDs are highly oxidized, supporting our hypothesized structure [16]. The empirical formula for B-CDs was calculated as $C_{1.3}H_{1.7}O$, discounting nitrogen due to its low percent composition. This formula shows a highly oxidized and hydrogenated structure from the treatment of carbon nanopowder with strong acids.

CNDs show a similar amount of carbon from both XPS and elemental

Table 3
Elemental composition of CDs as measured from XPS[16] and elemental analysis. The values for elemental analysis have been scaled to one hundred percent.

Technique	Sample	%C	%O	%N	%H
XPS	**B-CDs**	54.6	43.8	–	–
	CNDs	43.3	48.6	8.1	–
	Y-CDs	93.4	5.2	1.4	–
Elemental Analysis	**B-CDs**	46.7	46.4	1.9	5.0
	CNDs	45.3	33.0	17.4	4.3
	Y-CDs	53.6	26.0	14.2	6.2

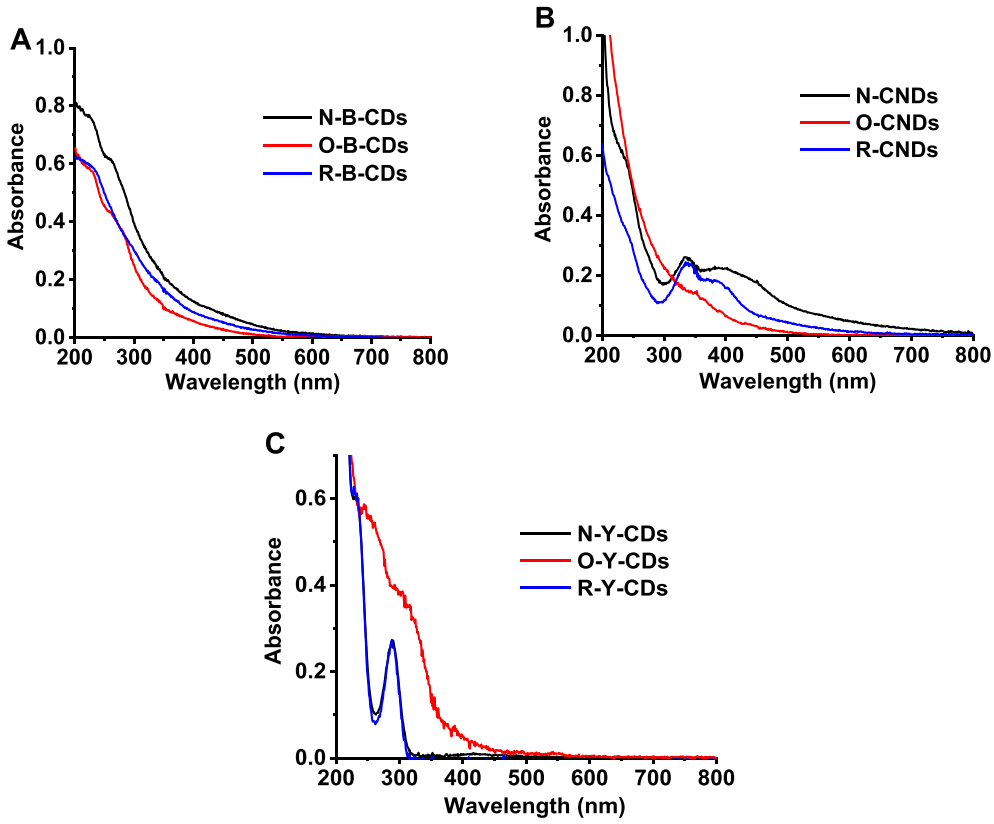

Fig. 2. UV–vis spectra for B-CDs (A), CNDs (B), and Y-CDs (C) in normal, oxidized, and reduced form. Optical pathlength was 1 cm.

analysis, however the amount of oxygen is decreased, and nitrogen is increased in elemental analysis. Since CNDs are formed through a bottom-up approach, oxidation of interior lattices is not favored since it hinders the formation of CNDs' 3D structure, but nitrogen is enhanced on the interior of CNDs due to the presence of s-triazine moieties and other nitrogen containing carbon lattices. The empirical formula of CNDs is calculated as $C_{3.2}H_{3.6}NO_{1.8}$. The groups observed from ToF-SIMS analysis line up well with these observed results. Groups such as $NH4^+$, $C_2H_4N^+$, and C_3NO^- have greater relative intensity for CNDs from SIMS data showing agreement between the three techniques.

The largest difference in Table 3 is related to Y-CDs. The discrepancy seen in these two datasets is most likely related to the process of formation for these CDs. Our previous work discussed how the oligomerization of citric acid and *o*-PDA, as well as *o*-PDA oligomerizing with itself, leads to a nanoscale structure with 3D arrangement. Due to the low molar ratio of citric acid (1:25 compared to *o*-PDA), the oxygen containing groups are more likely embedded in the core as the structure grows, and for this reason less oxygen presents on the surface. Both techniques show more carbon and less heteroatoms for Y-CDs compared to the other two particles, which is due to the gentler technique used for Y-CDs which limits oxidation. As previously mentioned, Y-CDs are more hygroscopic compared to other CDs and this may result in an inflated O/N ratio for these measurements.

3.3. Effect of oxidation/reduction on CDs' optical properties

To examine the role of surface groups on CDs' PL properties, they were treated with sodium hypochlorite and sodium borohydride to oxidize and reduce the surface of CDs, respectively. Fig. 2 shows the results of this modification on the absorption properties of CDs. B-CDs displays the least change which is unsurprising given the top-down approach they are prepared from, and the simplicity of the groups seen through ToF-SIMS. For CNDs, after oxidation there is a reduction or elimination of the longest wavelength peak (400 nm). Y-CDs is similar in that the peak at 420 nm is no longer distinct, however there is an increased tailing seen for the oxidized product indicating that the degree of disorder was increased, which is also supported by the broader peak seen at 280 nm compared to the normal and reduced forms [16].

The PL of each sample was also acquired and is presented in Figs. S6 and S7. In order to visualize differences between the different forms clearly, the data is presented in two ways in Fig. 3. First, emission wavelength is plotted versus excitation wavelength to clearly view any shifting that may occur after oxidation/reduction. Secondly, normalized emission intensity is plotted versus excitation wavelength to examine if the chemical modifications change the maximum excitation wavelength or relative intensities between different excitations. For B-CDs, the normal form exhibits broad emission peaks (Fig. S6), and these are present in the modified forms (oxidized and reduced), but there are also two distinct peaks around 450 and 510 nm. This separation of the peaks after modification indicates that there are two distinct electronic systems present as opposed to a single electronic structure with a broad range of vibrational transitions. Surprisingly, CNDs do not show much change after modification. There is a blue shifting for the emission peaks at short excitation wavelengths for R-CNDs, but this appears to be due to a change in relative intensity for emission after excitation at 325 nm and not to the origination of a new peak. A more important change can be seen in Fig. 3D which reveals that O-CNDs shows a higher relative intensity at excitations which are not the maximum (375 nm). This suggests that the maximum emission is sensitive to oxidation and is reduced relative to other emission peaks in CNDs after oxidation. Y-CDs shows the most change of all samples upon treatment with oxidant/reductant. O–Y-CDs displays completely different PL properties compared to N–Y-CDs as the excitation-independent emission peak at 565 nm has been completely eliminated and replaced with the more typical excitation-dependent spectra for CDs with maximum emission around 440 nm. R-Y-CDs does not show as dramatic a change, but there are still obvious

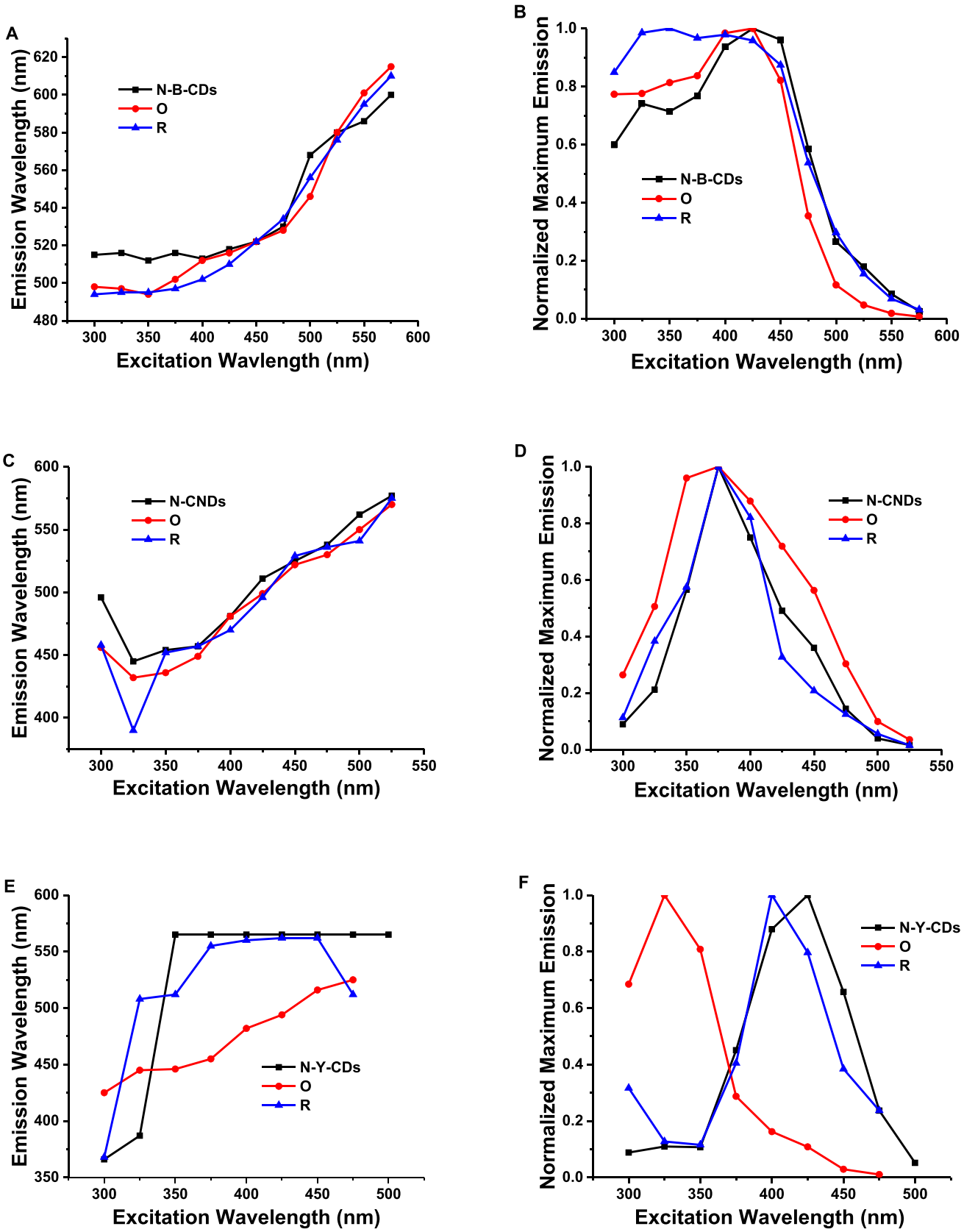

Fig. 3. Plot of emission maximum versus excitation wavelength for B-CDs (A), CNDs (C), and Y-CDs (E) and their oxidized and reduced forms. Plot of normalized emission intensity versus excitation wavelength for B-CDs (B), CNDs (D), and Y-CDs (F) and their oxidized and reduced forms.

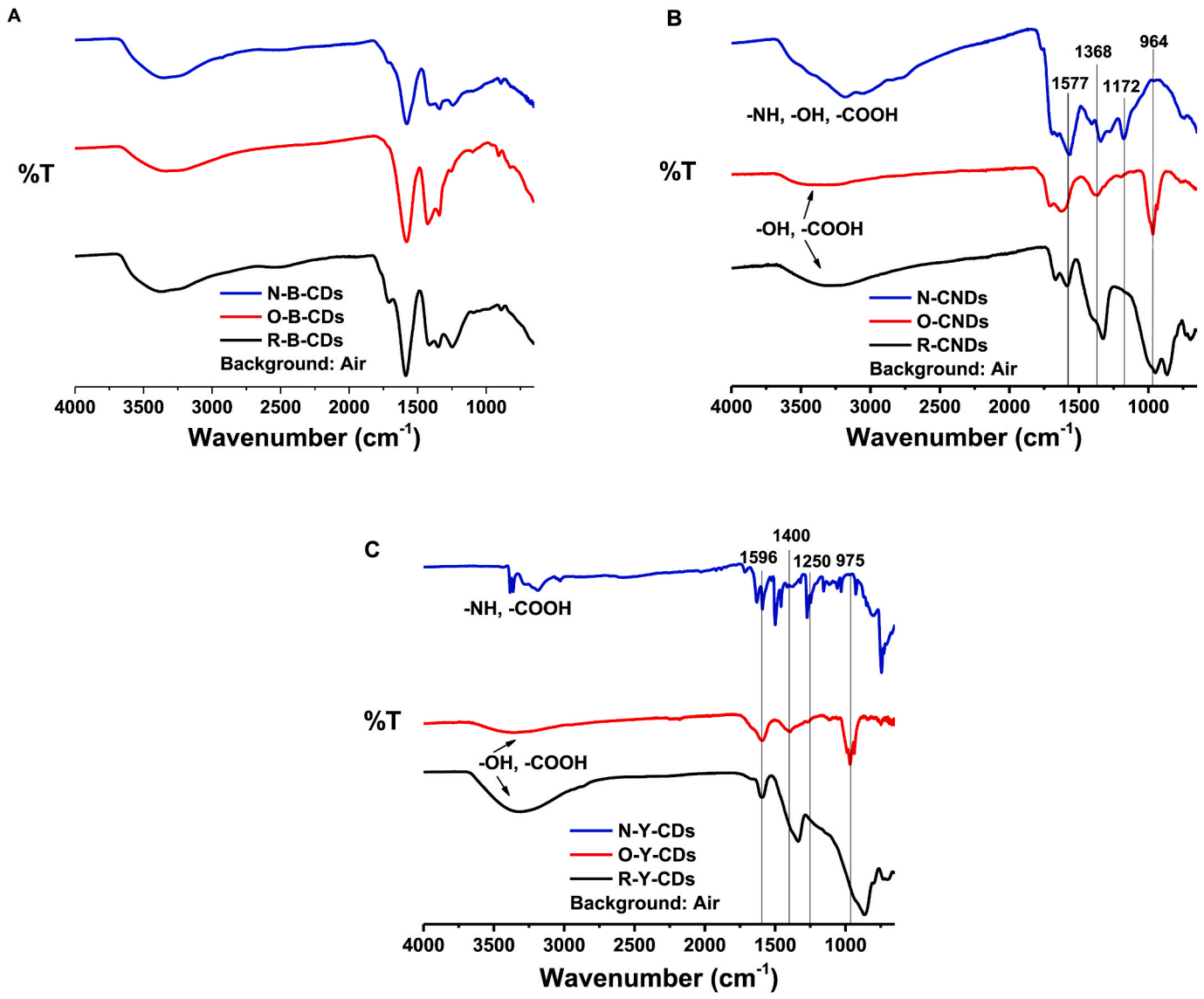

Fig. 4. FTIR spectra for B-CDs (A), CNDs (B), and Y-CDs (C) in normal, oxidized, and reduced form.

changes. Emission peaks in the UV region for R-Y-CDs are enhanced over N–Y-CDs, which possesses very minor peaks in the UV/blue region. Additionally, although the independent emission around 565 nm is retained in R-Y-CDs, a new emissive center around 510 nm has developed. The obvious and dramatic changes seen for Y-CDs supports the more organic/polymer-like structure proposed previously, but more information is needed for all samples to begin to ascribe structural meaning to the changes observed.

The FTIR spectra for each CDs sample in their normal and modified forms was recorded to monitor the change in structure during these reactions. Similar to the absorption and PL spectra, minimal changes were observed following oxidation or reduction of B-CDs (Fig. 4A). This illustrates the simplicity and stability of their structure. For CNDs and Y-CDs, there are some changes to be observed which are similar between the two particles. The peaks centered around 3200 cm^{-1} have become less sharp after oxidation/reduction indicating disappearance of the amine group and promotion of the alcohol group, respectively. For the oxidized samples, the peaks between 1550 and 1600 cm^{-1} have been shifted to slightly higher energies. This indicates hypochlorite attacked aromatic systems to break their rings and leave behind, in part, simple alkenes. The oxidized sample also shows promotion of the N–O bond between 1350 and 1400 cm^{-1} which is generated through the oxidation of primary amines. Both CNDs and Y-CDs show disappearance of peaks between 1000 and 1250 cm^{-1} upon oxidation and reduction. Peaks in this area may be attributed to many different groups, but a reasonable possibility for this disappearance is related to modification of C–O bonds which commonly absorb at different areas in this region depending on the form of the larger group. Oxidation of CNDs and Y-CDs gives rise to a peak just below 1000 cm^{-1} which can be attributed to the C═C bend which would be greatly enhanced after destruction of aromatic rings. Both of these samples also see an enhancement below 1000 cm^{-1} upon reduction which can be assigned to C–H bends, which are promoted after hydrogenation by borohydride.

There are multiple changes seen upon oxidation and reduction of these CDs systems, so some effort is needed to connect the modifications of optical and structural properties. B-CDs possesses little to no change in UV–Vis, PL, and FTIR spectra and so not much is learned except that the optical properties of B-CDs are not influenced by surface groups. CNDs displays more changes than is seen for B-CDs. Emission positions remain mostly unchanged, but there is an enhancement of relative intensity for the excitation wavelengths which are not the maximum (Fig. 3D). This indicates that the structure responsible for this emission is available on the surface of CNDs and is susceptible to oxidation. This suggests the importance of surface fluorophores for this reaction. This

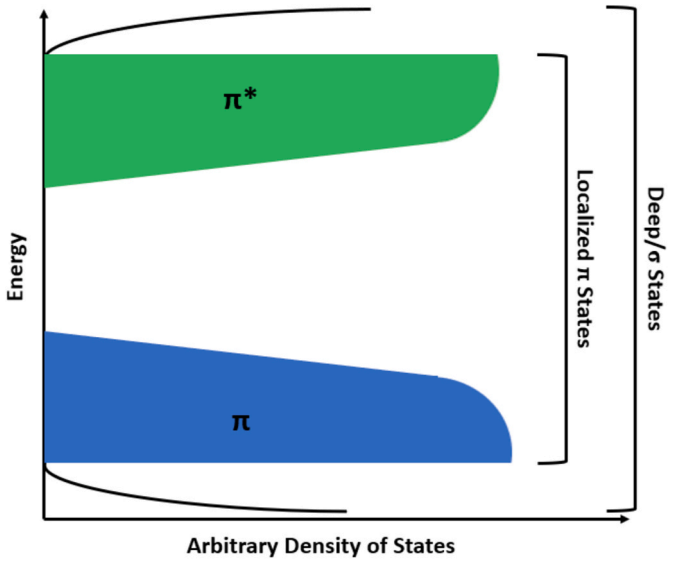

Fig. 5. Diagram of typical energy states for carbon materials and possible energy states for CDs.

possibility has been suggested for different systems involving citric acid and urea previously [39]. FTIR supports the possibility of loss of emission through breakdown of aromatic systems, as CNDs shows a shifting of the aromatic carbon peak to higher energies suggesting conversion of these groups to simple alkenes. The emission of CNDs is not completely depleted through either oxidation or reduction, so a dual mechanism is suggested, but it is clear that a factor in the PL of CDs is related to surface fluorophores. Y-CDs displays the most changes of any of the systems tested. The elimination of the peak around 565 nm through oxidation could be assumed to be through a similar process as discussed for CNDs, but what is interesting is the production of emission around 450 nm. This could possibly arise due to the oxidized product of the structural moiety responsible for 565 nm emission possessing emission in the blue region. This data clearly shows a different process for Y-CDs compared to B-CDs and CNDs.

3.4. Proposed PL mechanism for three CDs

To understand the potential pathway for CDs' emission properties it is necessary to first discuss the electronic structure of typical carbon materials (Fig. 5). In these materials, there are two main bands related to σ bonding and π bonding [29]. The states arising from σ bonding are very far apart in energy and not often relevant to electronic transitions. Conversely, the π bands are much closer in energy and transitions are commonly observed between them (blue and green states, Fig. 5) [30]. The states involved with this tailing are referred to as localized states since they are dependent on local disorder/structure defects. The presence of heteroatoms (e.g., oxygen and nitrogen) can also lead to an increased in the localized states [40]. This is especially important for CDs, because their maximum emission rarely comes from exciting at the wavelength of maximum absorption, but from the tailing region seen in the UV–vis spectrum as is the case for B-CDs and CNDs. With this in mind, we can now move to separately discuss the three CDs studied.

B-CDs' proposed emission mechanism can be considered relatively simple compared to CNDs and Y-CDs. For the precursor of B-CDs, carbon nanopowder, it is reasonable to suppose that the localized states do not play a significant role in the electronic structure. This is an amorphous powder but is pure carbon and fluorescence measurement confirmed that there is little signal when the nanopowder is dispersed in hexane. During the reaction to prepare B-CDs we are breaking off small particles and functionalizing them with oxygen [41]. This functionalization introduces localized states to the electronic structure and generates the PL properties observed. The excitation dependent emission is related to the variation of the states in different particles. Fig. 6 also may help to explain the difficulty in obtaining red emissive CDs, as the lowest energy transitions (between the tails of the localized states) are between low density states [42,43]. This concept of "localized states" is perhaps similar to the ill-defined (for CDs) "surface states", but the presence of these states should not be confined to the surface of the particle, especially for bottom-up approaches.

For CNDs, as discussed previously, surface fluorophores are likely contributing to the optical properties. However, even after oxidation of

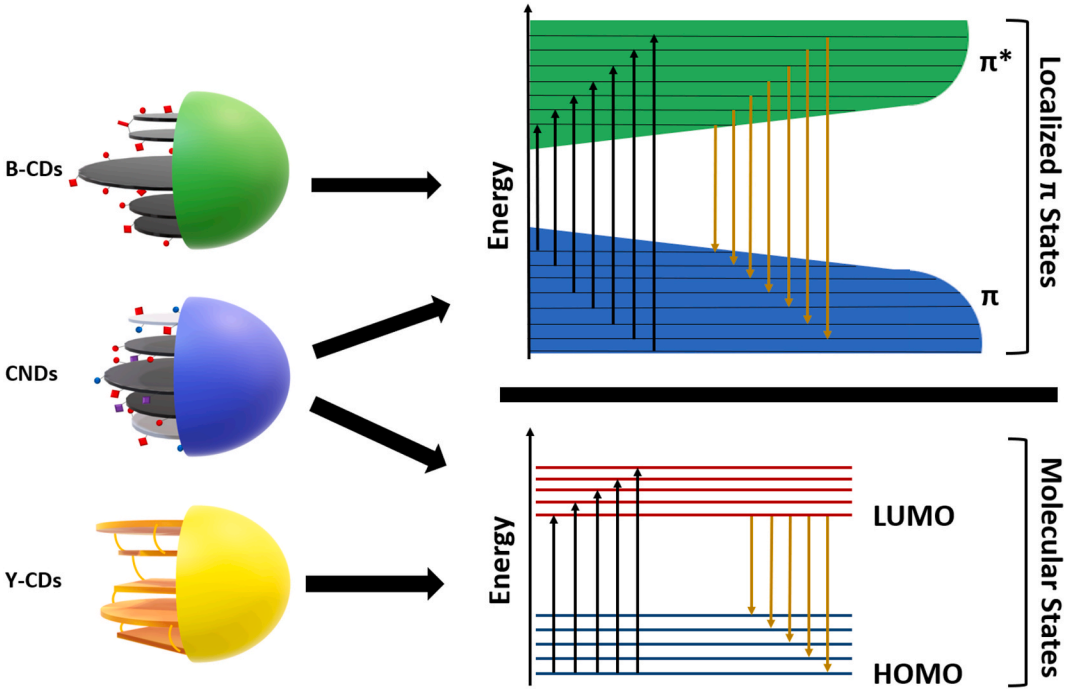

Fig. 6. Diagram attributing the two different emissive pathways to the three different CDs.

these fluorophores, much of the emission of CNDs remains. Therefore, we propose a dual mechanism for this system (Fig. 6). Fluorophores are generated in the preparation process which are then embedded in the structure for CNDs. These may help to dramatically increase the quantum yield of CNDs over B-CDs [5]. These fluorophores should generate fluorescence similar to if a dye was conjugated to CNDs post-reaction. However, there is also a process occurring which is similar to the one described above for B-CDs. With the formation of doped sp^2 carbon lattices during the preparation, the π bands form in the electronic structure and the presence of nitrogen and oxygen again help to create the localized states. This dual mechanism explains not only the excitation-dependence of CNDs, but also the bright emission seen at some excitation wavelengths.

For Y-CDs, the emission mechanism should be significantly different because mostly excitation-independent emission is observed. This emission shows sensitivity to reduction and is eliminated through oxidation. Excitation-independence suggests a molecular mechanism (Fig. 6), which would fit with the blue-shifted emission observed by reduction (through hydrogenation of a double bond) and the elimination of 565 nm emission through oxidation (through opening of aromatic rings). Additionally, tailing is observed for Y-CDs to a much smaller degree than the previous two CDs indicating that the localized states are much less important for this system. The identity of the species responsible for the emission of Y-CDs is unknown but may be related to an oligomer of *o*-PDA.

4. Conclusion

Understanding the surface structure of CDs is vital for optimization of several applications as well as understanding the interactions between these particles and biological systems. This work builds upon our previous work to provide a more detailed understanding of the structure of three important systems in our lab [15]. B-CDs have been shown to unsurprisingly contain mostly carbon structures with some structures functionalized with oxygen and nitrogen. CNDs possessed a combination of these carbon structures and small organic molecules which is consistent with the use of a bottom-up approach which uses enough energy to induce graphitization. Y-CDs possesses remnants of its precursors and larger, likely oligomeric structures which are most likely related to polymerization of the precursors. The comparison of ToF-SIMS data with XPS and elemental analysis results enables the inference of some groups' locations in CDs' structure. Finally, CDs structure were modified through oxidation/reduction in order to preliminary connect structural features with emissive properties and develop a proposed pathway of emission for the three studied systems. This work lays the foundation for a truly comprehensive model of CDs which can be used to understand the safety and potential for CDs' use in humans.

CRediT authorship contribution statement

Keenan J. Mintz: Conceptualization, Data curation, Formal analysis, Investigation, Methodology, Validation, Visualization, Writing – original draft, Writing – review & editing. **Claude Poleunis:** Conceptualization, Data curation, Formal analysis, Investigation, Validation, Writing – review & editing. **Braulio C.L.B. Ferreira:** Investigation, Methodology, Writing – review & editing. **Rachel Sampson:** Investigation, Methodology, Writing – review & editing. **Arnaud Delcorte:** Conceptualization, Data curation, Formal analysis, Investigation, Methodology, Validation, Writing – review & editing. **Roger M. Leblanc:** Conceptualization, Formal analysis, Funding acquisition, Supervision, Validation, Writing – review & editing.

Declaration of competing interest

The authors declare the following financial interests/personal relationships which may be considered as potential competing interests:

Roger Leblanc reports financial support was provided by University of Miami. Roger Leblanc reports a relationship with National Science Foundation that includes: funding grants.

Acknowledgement

R.M.L. would like to acknowledge the financial support of the National Science Foundation through awards #1809060 and #2041413. We would also like to thank Prof. Alberto Tagliaferro for his discussions with the authors on the concept of localized states in carbon materials.

Appendix A. Supplementary data

Supplementary data to this article can be found online at https://doi.org/10.1016/j.carbon.2024.118906.

References

[1] S. Iravani, R.S. Varma, Green synthesis, biomedical and biotechnological applications of carbon and graphene quantum dots, A review. Environ. Chem. Lett. 18 (2020) 703–727.
[2] Q. Wang, X. Huang, Y. Long, X. Wang, H. Zhang, R. Zhu, L. Liang, P. Teng, H. Zheng, Hollow luminescent carbon dots for drug delivery, Carbon 59 (2013) 192–199.
[3] S.D. Hettiarachchi, R.M. Graham, K.J. Mintz, Y. Zhou, S. Vanni, Z. Peng, R. M. Leblanc, Triple conjugated carbon dots as a nano-drug delivery model for glioblastoma brain tumors, Nanoscale 11 (13) (2019) 6192–6205.
[4] K. Hola, Y. Zhang, Y. Wang, E.P. Giannelis, R. Zboril, A.L. Rogach, Carbon dots—Emerging light emitters for bioimaging, cancer therapy and optoelectronics, Nano Today 9 (5) (2014) 590–603.
[5] P.Y. Liyanage, R.M. Graham, R.R. Pandey, C.C. Chusuei, K.J. Mintz, Y. Zhou, J. K. Harper, W. Wu, A.H. Wikramanayake, S. Vanni, Carbon nitride dots: a selective bioimaging nanomaterial, Bioconj. Chem. 30 (1) (2018) 111–123.
[6] J. Di, J. Xia, X. Chen, M. Ji, S. Yin, Q. Zhang, H. Li, Tunable oxygen activation induced by oxygen defects in nitrogen doped carbon quantum dots for sustainable boosting photocatalysis, Carbon 114 (2017) 601–607.
[7] Y. Zhou, E.M. Zahran, B.A. Quiroga, J. Perez, K.J. Mintz, Z. Peng, P.Y. Liyanage, R. R. Pandey, C.C. Chusuei, R.M. Leblanc, Size-dependent photocatalytic activity of carbon dots with surface-state determined photoluminescence, Appl. Catal. B Environ. 248 (2019) 157–166.
[8] K.J. Mintz, B. Guerrero, R.M. Leblanc, Photoinduced electron transfer in carbon dots with long-wavelength photoluminescence, J. Phys. Chem. C 122 (51) (2018) 29507–29515.
[9] M.L. Liu, B.B. Chen, C.M. Li, C.Z. Huang, Carbon dots: synthesis, formation mechanism, fluorescence origin and sensing applications, Green Chem. 21 (3) (2019) 449–471.
[10] J. Yeagle, Nanotechnology and the FDA. Va, JL & Tech. 12 (2007) 1.
[11] K.J. Mintz, Y. Zhou, R.M. Leblanc, Recent development of carbon quantum dots regarding their optical properties, photoluminescence mechanism, and core structure, Nanoscale 11 (11) (2019) 4634–4652.
[12] C. Xia, S. Zhu, T. Feng, M. Yang, B. Yang, Evolution and synthesis of carbon dots: from carbon dots to carbonized polymer dots, Adv. Sci. 6 (23) (2019) 1901316–1901338.
[13] M.T. Paloncýová, M. Langer, M. Otyepka, Structural dynamics of carbon dots in water and n, n-dimethylformamide probed by all-atom molecular dynamics simulations, J. Chem. Theory Comput. 14 (4) (2018) 2076–2083.
[14] S. Tajik, Z. Dourandish, K. Zhang, H. Beitollahi, Q. Van Le, H.W. Jang, M. Shokouhimehr, Carbon and graphene quantum dots: a review on syntheses, characterization, biological and sensing applications for neurotransmitter determination, RSC Adv. 10 (26) (2020) 15406–15429.
[15] W. Shi, Q. Han, J. Wu, C. Ji, Y. Zhou, S. Li, L. Gao, R.M. Leblanc, Z. Peng, Synthesis mechanisms, structural models, and photothermal therapy applications of top-down carbon dots from carbon powder, graphite, graphene, and carbon nanotubes, Int. J. Molec. Sci. 23 (3) (2022) 1456.
[16] K.J. Mintz, M. Bartoli, M. Rovere, Y. Zhou, S.D. Hettiarachchi, S. Paudyal, J. Chen, J.B. Domena, P.Y. Liyanage, R. Sampson, A deep investigation into the structure of carbon dots, Carbon 173 (2021) 433–447.
[17] Q. Xu, W. Cai, M. Zhang, R. Su, Y. Ye, Y. Li, L. Zhang, Y. Guo, Z. Yu, S. Li, Photoluminescence mechanism and applications of Zn-doped carbon dots, RSC Adv. 8 (31) (2018) 17254–17262.
[18] C. Russo, A. Carpentieri, A. Tregrossi, A. Ciajolo, B. Apicella, Blue, green and yellow carbon dots derived from pyrogenic carbon: structure and fluorescence behaviour, Carbon 201 (2023) 900–909.
[19] A. Delcorte, V. Delmez, C. Dupont-Gillain, C. Lauzin, H. Jefford, M. Chundak, C. Poleunis, K. Moshkunov, Large cluster ions: Soft local probes and tools for organic and bio surfaces, Phys. Chem. Chem. Phys. 22 (31) (2020) 17427–17447.
[20] A. Delcorte, C. Leblanc, C. Poleunis, K. Hamraoui, Computer simulations of the sputtering of Metallic, organic, and metal–organic surfaces with Bi n and C60 Projectiles, J. Phys. Chem. C 117 (6) (2013) 2740–2752.

[21] D.I. Patel, C.G. McKenas, D. Shah, M.R. Lockett, J.E. Patterson, M.R. Linford, Multi-instrument characterization of carbon nanodot materials, Vacuum Technol. Coating (2018) 24–28.
[22] J.C.S. Ana, D.H. Camacho, Preparation and characterization of carbon nanodots from natural polysaccharides and its application as photo sensitizer in solar sell, Research Congress DLSU (2019).
[23] A.P. Demchenko, C, Excitons in Carbonic Nanostructures, vol. 5, 2019, p. 71, 4.
[24] X. Yao, R.E. Lewis, C.L. Haynes, Synthesis processes, photoluminescence mechanism, and the toxicity of amorphous or polymeric carbon dots, Acc. Chem. Res. 55 (23) (2022) 3312–3321.
[25] C. He, P. Xu, X. Zhang, W. Long, The synthetic strategies, photoluminescence mechanisms and promising applications of carbon dots: current state and future perspective, Carbon 186 (2022) 91–127.
[26] W.P. Kasprzyk, T. Świergosz, P.P. Romańczyk, J. Feldmann, J. Stolarczyk, The role of molecular fluorophores in photoluminescence of carbon dots derived from citric acid: current state of the art and future perspectives, Nanoscale 14 (2022) 14368–14384.
[27] B. Wang, S. Lu, The light of carbon dots: from mechanism to applications, Matter 5 (1) (2022) 110–149.
[28] V. Heine, Theory of surface states, Phys. Rev. 138 (6A) (1965) A1689.
[29] D. Dasgupta, F. Demichelis, C. Pirri, A. Tagliaferro, π bands and gap states from optical absorption and electron-spin-resonance studies on amorphous carbon and amorphous hydrogenated carbon films, Phys. Rev. B 43 (3) (1991) 2131.
[30] G. Fanchini, S. Ray, A. Tagliaferro, Density of electronic states in amorphous carbons, Diamond Rel. Mater. 12 (3–7) (2003) 891–899.
[31] Q. Lou, Q. Ni, C. Niu, J. Wei, Z. Zhang, W. Shen, C. Shen, C. Qin, G. Zheng, K. Liu, Carbon nanodots with nearly unity fluorescent efficiency realized via localized excitons, Adv. Sci. 9 (30) (2022) 2203622.
[32] J. Zang, F. Jiao, J. Wei, Q. Lou, G. Zheng, C. Shen, Y. Deng, E. Soheyli, R. Sahraei, X. Yang, Carbon nanodot with highly localized excitonic emission for efficient luminescent solar concentrator, Nanophoton 12 (21) (2023) 4117–4126.
[33] S. Li, L. Wang, C.C. Chusuei, V.M. Suarez, P.L. Blackwelder, M. Micic, J. Orbulescu, R.M. Leblanc, Nontoxic carbon dots potently inhibit human insulin fibrillation, Chem. Mater. 27 (5) (2015) 1764–1771.
[34] P.Y. Liyanage, Y. Zhou, A.O. Al-Youbi, A.S. Bashammakh, M.S. El-Shahawi, S. Vanni, R.M. Graham, R.M. Leblanc, Pediatric glioblastoma target-specific efficient delivery of gemcitabine across the blood–brain barrier via carbon nitride dots, Nanoscale 12 (14) (2020) 7927–7938.
[35] Y. Zhou, K. Mintz, C. Oztan, S. Hettiarachchi, Z. Peng, E. Seven, P. Liyanage, S. De La Torre, E. Celik, R. Leblanc, Embedding carbon dots in superabsorbent polymers for additive manufacturing, Polymers 10 (8) (2018) 921.
[36] Y. Zhou, P.Y. Liyanage, D. Devadoss, L.R.R. Guevara, L. Cheng, R.M. Graham, H. S. Chand, A.O. Al-Youbi, A.S. Bashammakh, M.S. El-Shahawi, Nontoxic amphiphilic carbon dots as promising drug nanocarriers across the blood–brain barrier and inhibitors of β-amyloid, Nanoscale 11 (46) (2019) 22387–22397.
[37] Y. Zhou, N. Kandel, M. Bartoli, L.F. Serafim, A.E. ElMetwally, S.M. Falkenberg, X. E. Paredes, C.J. Nelson, N. Smith, E. Padovano, Structure-activity relationship of carbon nitride dots in inhibiting Tau aggregation, Carbon 193 (2022) 1–16.
[38] I. Papagiannouli, M. Patanen, V. Blanchet, J.D. Bozek, M. de Anda Villa, M. Huttula, E. Kokkonen, E. Lamour, E. Mevel, E. Pelimanni, Depth profiling of the chemical composition of free-standing carbon dots using X-ray photoelectron spectroscopy, J. Phys. Chem. C 122 (26) (2018) 14889–14897.
[39] J. Schneider, C.J. Reckmeier, Y. Xiong, M. von Seckendorff, A.S. Susha, P. Kasák, A. L. Rogach, Molecular fluorescence in citric acid-based carbon dots, J. Phys. Chem. C 121 (3) (2017) 2014–2022.
[40] L. Tang, R. Ji, X. Li, K.S. Teng, S.P. Lau, Energy-level structure of nitrogen-doped graphene quantum dots, J. Mater. Chem. C 1 (32) (2013) 4908–4915.
[41] C. Li, X. Chen, L. Shen, N. Bao, Revisiting the oxidation of graphite: reaction mechanism, chemical stability, and structure self-regulation, ACS Omega 5 (7) (2020) 3397–3404.
[42] H. Ding, X.-X. Zhou, J.-S. Wei, X.-B. Li, B.-T. Qin, X.-B. Chen, H.-M. Xiong, Carbon dots with red/near-infrared emissions and their intrinsic merits for biomedical applications, Carbon 167 (2020) 322–344.
[43] K.J. Mintz, E.K. Cilingir, G. Nagaro, S. Paudyal, Y. Zhou, D. Khadka, S. Huang, R. M. Graham, R.M. Leblanc, Development of red-emissive carbon dots for bioimaging through a building block approach: fundamental and applied studies, Bioconj. Chem. 33 (1) (2021) 226–237.